Neutrophil extracellular traps as a unique target in the treatment of chemotherapy-induced peripheral neuropathy

Chao-Yu Wang,[a,h] Tong-Tong Lin,[a,h] Liang Hu,[a,h] Chen-Jie Xu,[b,h] Fan Hu,[a] Li Wan,[a] Xing Yang,[a] Xue-Feng Wu,[c] Xiao-Tao Zhang,[d,e] Yan Li,[d,f] Hao-Yuan Yin,[g] Chun-Yi Jiang,[a,*] Hong-Liang Xin,[g,**] and Wen-Tao Liu[a,***]

[a]Jiangsu Key Laboratory of Neurodegeneration, Department of Pharmacology, Nanjing Medical University, Nanjing, Jiangsu, China
[b]Department of Anesthesiology and Pain, Nanjing First Hospital, Nanjing Medical University, Nanjing, Jiangsu, China
[c]State Key Laboratory of Pharmaceutical Biotechnology, School of Life Sciences, Nanjing University, Nanjing, Jiangsu, China
[d]Department of Oncology, Shandong Provincial Qianfoshan Hospital, Shandong University, Jinan, Shandong, China
[e]Department of Radiation Oncology, Qingdao Central Hospital, Qingdao, Shandong, China
[f]Department of Oncology, Shandong Provincial Qianfoshan Hospital, The First Hospital Affiliated with Shandong First Medical University, Jinan, Shandong, China
[g]Department of Pharmaceutics and Key Laboratory of Cardiovascular & Cerebrovascular Medicine, School of Pharmacy, Nanjing Medical University, Nanjing Jiangsu, China

eBioMedicine
2023;90: 104499
Published Online xxx
https://doi.org/10.1016/j.ebiom.2023.104499

Summary

Background Chemotherapy-induced peripheral neuropathy (CIPN) is a severe dose-limiting side effect of chemotherapy and remains a huge clinical challenge. Here, we explore the role of microcirculation hypoxia induced by neutrophil extracellular traps (NETs) in the development of CIPN and look for potential treatment.

Methods The expression of NETs in plasma and dorsal root ganglion (DRG) are examined by ELISA, IHC, IF and Western blotting. IVIS Spectrum imaging and Laser Doppler Flow Metry are applied to explore the microcirculation hypoxia induced by NETs in the development of CIPN. Stroke Homing peptide (SHp)-guided deoxyribonuclease 1 (DNase1) is used to degrade NETs.

Findings The level of NETs in patients received chemotherapy increases significantly. And NETs accumulate in the DRG and limbs in CIPN mice. It leads to disturbed microcirculation and ischemic status in limbs and sciatic nerves treated with oxaliplatin (L-OHP). Furthermore, targeting NETs with DNase1 significantly reduces the chemotherapy-induced mechanical hyperalgesia. The pharmacological or genetic inhibition on myeloperoxidase (MPO) or peptidyl arginine deiminase-4 (PAD4) dramatically improves microcirculation disturbance caused by L-OHP and prevents the development of CIPN in mice.

Interpretation In addition to uncovering the role of NETs as a key element in the development of CIPN, our finding provides a potential therapeutic strategy that targeted degradation of NETs by SHp-guided DNase1 could be an effective treatment for CIPN.

Funding This study was funded by the National Natural Science Foundation of China 81870870, 81971047, 81773798, 82271252; Natural Science Foundation of Jiangsu Province BK20191253; Major Project of "Science and Technology Innovation Fund" of Nanjing Medical University 2017NJMUCX004; Key R&D Program (Social Development) Project of Jiangsu Province BE2019732; Nanjing Special Fund for Health Science and Technology Development YKK19170.

Keywords: Chemotherapy-induced peripheral neuropathy; Neutrophil extracellular traps; Microcirculatory disturbance; SHp-DNase1

Abbreviations: CIPN, Chemotherapy-induced peripheral neuropathy; DNase 1, Deoxyribonuclease 1; DRG, Dorsal Root Ganglion; HIF-1α, Hypoxia Inducible Factor-1α; LPS, Lipopolysaccharide; MMP, Matrix Metalloproteinase; MPO, Myeloperoxidase; NE, Neutrophil Elastase; NETs, Neutrophil Extracellular Traps; PAD4, Peptidyl arginine deiminase-4; SHp, Stroke Homing peptide

*Corresponding author.
**Corresponding author.
***Corresponding author.
E-mail addresses: jcy@njmu.edu.cn (C.-Y. Jiang), xhl@njmu.edu.cn (H.-L. Xin), painresearch@njmu.edu.cn (W.-T. Liu).
[h]These authors contributed equally to this work.

Research in context

Evidence before this study

Oxaliplatin is a platinum-derivative chemotherapeutic agent used to treat patients with digestive tumors. Neurotoxicity is the most severe adverse effect of oxaliplatin. However, the mechanisms underlying OIPN pathogenesis are not fully understood. Several factors, such as mitochondrial damage, neuroinflammation, oxidative stress and degeneration of peripheral nerves have been proposed as determinants of OIPN. It was reported that gut microbes could promote the development of CIPN. Our previous study demonstrated that TLR4-p38-TF-HIF-1α axis played a pivotal role in the pathological process of CIPN. The emergence of bacteria in plasma could promote NETosis and the association between NETs and thrombus formation is well studied.

Added value of this study

We identified that microcirculation hypoxia induced by neutrophil extracellular traps is essential for the development of CIPN. Oxaliplatin induced robust reactive oxygen species generation and promoted NETs formation via MPO/NE and PAD4 pathways. Targeting NETs with DNase1 significantly reduced the chemotherapy-induced mechanical hyperalgesia. Notably, CIPN in mice was almost abolished after the administration of novel Stroke Homing peptide (SHp)-guided DNase1.

Implications of all the available evidence

Our study uncovers the critical role of NETs contributing to the development of CIPN, and targeted degradation of NETs by SHp-guided DNase1 would be an effective treatment for CIPN.

Introduction

As a consequence of advances in cancer diagnose and treatment, long-term quality of life is an increasing important issue.[1] Therefore, neurotoxicity resulted from chemotherapeutic agents is critical to cancer survivors. It was reported that 48% of patients under chemotherapy, such as platinum, vinca alkaloids or taxanes, suffer from chemotherapy-induced peripheral neuropathy (CIPN).[2–4] The symptoms of CIPN include devastating neuropathic pain lasting from months to years, which may lead to permanent disability. Peripheral nerve degeneration or small fibre neuropathy is generally accepted as the underlying mechanism in the development of CIPN. Mitochondrial dysfunction, oxidative stress, altered action of ion channels, cytokines and chemokines have been also highlighted as key players in the pathophysiology of CIPN. Recent evidence has contributed to clarify the determinant role of thromboembolic events in cancer patients. It leads to the development of venous thromboembolism (VTE) which is a frequent and potentially life-threatening complication.[5] However, little is known whether there is a relationship between CIPN and the disturbances of circulation caused by thrombosis. We have found that hirudin, a classical anticoagulant, partially alleviates mechanical hyperalgesia with improvement of blood flow in mice treated with oxaliplatin (L-OHP), a platinum-based antineoplastic agent (Supplementary Fig. S1). It implies an alternative mechanism in triggering thrombosis during the development of CIPN under chemotherapeutics treatment.

However, the causes of microcirculation disturbance-induced CIPN are not fully clarified. In this study, our results describe that the formation of neutrophil extracellular traps (NETs) is triggered with the release of granule proteins and chromatin by neutrophils in peripheral nervous systems after chemotherapy. NETs, as a scaffold, could trigger tissue factor pathway to promote thrombosis.[6] Our previous studies found that chemotherapy increases the expression of tissue factor (TF) and activates matrix metalloproteinase (MMP)-9/2 in sciatic nerve.[7] Furthermore, L-OHP induces the expression of HIF-1α, which implies the emergence of ischemia and hypoxia under drug remedy.[7] A large number of clinical research report another side effect of chemotherapy, neutropenia, which is also one of the common side effects caused by platinum drugs.[8,9] Taken together, we suppose that NETs may play a critical role in the pathogenesis of CIPN via microcirculation disturbance.

In this study, we reveal the critical role of NETs in the chemotherapy-induced mechanical hyperalgesia in mice with a variety of strategies including small molecular inhibitor, Pad4 knockout mice, and SHp-deoxyribonuclease 1 (DNase1).

Methods

Patients and clinical data

The study was approved by the institutional review board of Nanjing First Hospital registered under KY20171228-KS-01, and all methods were carried out in accordance with relevant guidelines and regulations. A total of 64 patients and 32 healthy adult volunteers were enrolled in the study. The baseline characteristics of the patients without chemotherapy are summarized in Supplementary Table S1. The median (range) of the patients was 69.5 (50–83) years, and 43.75% of patients were female. The baseline characteristics of the patients treated with chemotherapy are summarized in Supplementary Table S2. The median (range) age of the

patients was 65 (34–83) years, and 40.6% of patients were female. The median (range) of total oxaliplatin was 775 mg/m^2. The inclusion criteria were as follows: 1) Karnofsky score >50%; 2) expected survival time >3 months; 3) at least one measurable lesion confirmed by CT or PET-CT; 4) normal bone marrow reserve and heart, liver and kidney function; 5) no serious complications and no second primary tumors; 6) oxaliplatin or oxaliplatin combination therapy; 7) All patients had different degrees of functional impairment (difficulty grasping, walking, wearing clothes, and inability to wear closed shoes). Moreover, pain intensity was measured by the visual analog scale (VAS). VAS is most commonly a straight 100-mm line, without demarcation, that has the words "no pain" at the left-most end and "worst pain imaginable" (or something similar) at the right-most end. Patients are instructed to place a mark on the line indicating the amount of pain that they feel at the time of the evaluation. The distance of this mark from the left end is then measured, and this number is used as a numeric representation of the severity of the patient's pain. The median (range) of VAS was 5 (2–10). Peripheral blood samples from cancer patients with/without chemotherapy (chemotherapy regimen containing oxaliplatin) were provided by Nanjing First Hospital, and healthy donor whole blood samples were provided by the University of Nanjing Medical University. The sample collection processes for both followed approved institutional review board protocols with patients providing informed consent.

Ethics statement

All procedures were strictly performed in accordance with the regulations of the ethics committee of the International Association for the Study of Pain and the Guide for the Care and Use of Laboratory Animals (The Ministry of Science and Technology of China, 2006). All animal experiments were approved by the Nanjing Medical University Animal Care and Use Committee (No. IACUC-1903031) and were designed to minimize suffering and the number of animals used. All animal experiments complied with the ARRIVE (Animal Research: Reporting of In Vivo Experiments) guidelines (https://arriveguidelines.org).

Animals and oxaliplatin-induced peripheral neuropathy model

At present, pain research on animal models usually have been conducted on male rodents. Adult male ICR mice and C57BL/6J mice (20–25 g wild type) were purchased from the Animal Core Facility of Nanjing Medical University, Nanjing, China. *Pad4*$^{-/-}$ mice on a C57BL/6J background were purchased from The Jackson Laboratory. Animals were housed five per cage under pathogen-free conditions with soft bedding under controlled temperature (22 ± 2 °C) and photoperiods (12:12-h light–dark cycle). The animals were habituated to these conditions for at least 2 days before starting experiments. Animals were randomly divided into groups. The sample size was designed on prior experience and to be limited to the minimal as scientifically justified. For each group of experiments, the animals were matched by age and body weight. Intraperitoneal injections of oxaliplatin (3 mg/kg) (H20093167, Qilu Pharmaceutical (Hainan) Co., Ltd.) were conducted from day 1 to day 5 to establish animal models of oxaliplatin-induced peripheral neuropathy. For the assessment of mechanical hyperalgesia, mice were administered the protein arginine deiminase 4 (PAD4) inhibitor Cl-amidine (S8141, Selleck; 10 mg/kg, i.p.) or the myeloperoxidase (MPO) inhibitor PF-1355 (HY-100873, MedChemExpress; 50 mg/kg, i.p.) one day before L-OHP administration until the end of 14 days (n = 8). And mice were injected with 150U i.v. DNase1 (D5025, Sigma) from the first day of modeling to the 14th day or from the sixth day of modeling to the 14th day (n = 8). Animals were used and monitored daily for behavioral tests. Serum samples and various tissues were collected at the indicated time points for ELISA analyses. DRG tissues were isolated and stored at –80 °C until Western blot analyses (n = 3 per group). In addition, the colon samples were dissected and fixed in 4% paraformaldehyde (PFA) fixative solution for HE staining and the DRG of the mice were dissected and fixed in 4% paraformaldehyde (PFA) fixative solution for immunofluorescence assay.

Behavior

Animals were habituated to the testing environment daily for at least 2 days before baseline testing. Mechanical sensitivity was detected by Von Frey hairs before L-OHP administration every morning. Animals were placed in boxes set on an elevated metal mesh floor and were allowed 30 min for habituation before testing. The plantar surface of each hind paw was stimulated with a series of Von Frey hairs with logarithmically incrementing stiffness perpendicular to the plantar surface. Each mouse was tested three times, and the average of the threshold was measured. Behavioral tests were performed blindly.

Hematoxylin and eosin staining

The colon samples were immersed in 4% paraformaldehyde for 4 h and transferred to 70% ethanol. Then, the samples were dehydrated through a serial alcohol gradient and embedded in paraffin wax blocks. Before immunostaining, colon tissue sections were dewaxed in xylene, rehydrated through decreasing concentrations of ethanol, and washed in PBS. Then, the sections were stained with hematoxylin and eosin. After staining, sections were dehydrated through increasing concentrations of ethanol and xylene. Finally, images were obtained using fluorescence microscopy (LEICA DM2500).

Lower limb blood flow measurement

Lower limb blood flow was measured using Laser Doppler Flow Metry (LDF). Specifically, a computer-controlled optical scanner was used to direct a low-power laser beam over the exposed lower limb. Concurrently, the scanner head was positioned parallel to the exposed lower limb at a distance of approximately 20 cm. Subsequently, a color-coded image that denoted the specific relative perfusion level was displayed on the video monitor. Blood flow values were recorded and evaluated by the moor FLPIR view V40 program (Gene & I Scientific. Ltd).

MPO activity assay

DRG was homogenized in 50 mM potassium phosphate buffer, centrifuged, and suspended in 0.5% cetytrimethylammonium bromide in potassium phosphate buffer. The suspensions were sonicated for 30 s with three freeze–thaw cycles in liquid nitrogen. After centrifugation, 40 mL of supernatant was incubated with 100 μL tetramethylbenzidine solution, and the reaction was stopped with 100 μL 2 N HCl. The optical density was measured at 450 nm.

IVIS Spectrum imaging

Cy5-NHS-labeled ischemic homing peptide was used for IVIS Spectrum imaging. For the imaging study, 2 h after intravenous administration, an IVIS Spectrum imaging system (PerkinElmer) was employed to capture ischemic images of mice. The sciatic nerves were fixed in 4% paraformaldehyde and then imaged.

Gelatin zymography assay

Animals were anesthetized deeply with 1% pentobarbital sodium (100 mg/kg, i.p.). DRGs were rapidly dissected and homogenized in 1% NP40 lysis buffer. DRG protein (300–500 μg per lane) was loaded into the wells of precast gels (8% polyacrylamide gels containing 0.1% gelatin). After electrophoresis, each gel was incubated with 50 ml of developing buffer for 48 h (37.5 °C) in a shaking bath. Then, the gels were stained with Coomassie brilliant blue (1%, with 10% acetic acid, 10% isopropyl alcohol, diluted with ddH2O).

ELISA

Levels of IL-6 and TNF-α were evaluated by ELISA Kits (R&D Biosystems, Minneapolis, MN) according to the manufacturer's instructions. The lower detection limit was 1.8 pg/mL for IL-6 and 7.2 pg/mL for TNF-α. The assay plates were read at 450 nm and 540 nm. All samples were run in duplicate.

LPS (endotoxin) assay

All materials used for both sample preparation and testing were pyrogen free. Lipopolysaccharide (LPS) concentrations in serum and tissue homogenate were evaluated by an endotoxin assay based on a limulus amebocyte extract with a chromogenic limulus amebocyte lysate (LAL) assay (Pierce LAL Chromogenic Endotoxin Quantitation Kit, 88282, Thermo Fisher Scientific). Samples were diluted in pyrogen-free water and heated to 70 °C for 10 min to inactivate inhibitor agents that could interfere with the assay. All samples were tested in duplicate. The endotoxin content was expressed as endotoxin units per milliliter (EU/mL) or endotoxin units per 100 mg of tissue.

Flow cytometry

Peripheral blood was subjected to red blood cell lysis buffer (ACK Lysis Buffer, A10492-01, Gibco). Cells were washed with phosphate-buffered saline (PBS) containing 1% bovine serum albumin (BSA) and incubated with APC-conjugated antibody to CD11b, PE-conjugated antibody to CD45 and Alexa Fluor 488-conjugated antibody to Ly6G at room temperature (22–24 °C) for 30 min. All samples were acquired by a BD FACSVerse flow cytometer. Data were analysed with Flowjo software. The information on antibodies applied in this study referred to Reagent Validation.

Immunofluorescence assay

After deep anesthesia by intraperitoneal injection of 1% pentobarbital sodium (100 mg/kg, i.p.), the animal was perfused transcardially with normal saline followed by 4% paraformaldehyde in 0.1 M PB, pH 7.4, each for 20 min. Then, the lumbar 5 DRG was dissected out and postfixed in 4% paraformaldehyde. The embedded blocks were sectioned as 10 μm thick. Blocking was achieved using 1% normal donkey serum (017-000-121, Jackson ImmunoResearch) and 0.1% Triton-X in phosphate-buffered solution (PBS) for 1 h. The specimens were incubated with anti-NE antibody, anti-MPO antibody, or CD31 antibody overnight at 4 °C. The secondary antibodies used were as follows: Alexa Fluor 488-conjugated donkey anti-rabbit, Alexa Fluor 647-conjugated donkey anti-goat, and Alexa Fluor 594-conjugated donkey anti-mouse for 2 h at room temperature. After washing out three times with PBS, the samples were studied under a confocal laser scanning microscope (Zeiss LSM880 with Airyscan) for morphologic details of the immunofluorescence staining. Examination was blindly carried out. The information on antibodies applied in this study referred to Reagent Validation.

Neutrophil isolation

Mice were euthanized using the institution's animal care committee-approved protocol, and the animal surface was sprayed with 75% ethanol. Cut off the muscles from the lower extremities using scissors and carefully dislocate the acetabulum from the hip joint while avoiding breaking the femur head. Remove the remaining muscles from the femur and tibia using a scalpel and scissors and separate the femur from the

tibia at the knee joint exercising care to avoid breaking the bone ends. Place the bones in a Petri dish containing ice-cold RPMI 1640 supplemented with 10% FBS and 1% penicillin/streptomycin. The following steps were performed under a tissue culture hood. Extra precautions should be taken to maintain strict sterile techniques to avoid neutrophil activation. Rinse each bone with 75% ethanol followed by three subsequent washes in ice-cold sterile PBS (within Petri dishes) to rinse off the ethanol from the surface of the bones. Inside a clean sterile Petri dish, cut off the epiphyses of the bones and keep them aside. Use a 25-gauge needle and a 12-cc syringe filled with RPMI supplemented with 10% FBS and 2 mM EDTA and flush the bone marrow cells from both ends of the bone shafts onto a 50 ml screw top Falcon tube fitted with a 100 μm filter. Centrifuge at 1400 rpm for 7 min at 4 °C. The red blood cells were lysed by resuspending the cell pellet in 20 ml of 0.2% NaCl for approximately 20 s followed by the addition of 20 ml of 1.6% NaCl. Neutrophils were separated by density gradient centrifugation. Bone marrow cells were counted and resuspended in 1 ml of ice-cold sterile PBS. Add 3 ml of Histopaque 1119 (density, 1.119 g/ml, Sigma) in a 15-ml conical tube. Overlay 3 ml of Histopaque 1077 (density, 1.077 g/ml, Sigma) on the 3 ml of Histopaque 1119. Overlay of the bone marrow cell suspension on top of Histopaque 1077. Centrifuge for 30 min at 2000 rpm at 25 °C without braking. Neutrophils were collected at the interface of the Histopaque 1119 and Histopaque 1077 layers. The collected neutrophils were washed twice with RPMI 1640 1× supplemented with 10% FBS and 1% penicillin/streptomycin and centrifuged at 1400 rpm for 7 min at 4 °C.

In vitro NET assay

For immunofluorescence staining, freshly isolated polymorphonuclear neutrophils (PMNs) from the bone marrow were seeded on poly-D-lysine-coated cover slips and allowed to adhere. Cells were treated with NAC (100 μm) (HY-B0215, MedChemExpress) and TAK242 (10 μm) (HY-11109, MedChemExpress) for 3 h and then stimulated with LPS (10 ng/mL) + L-OHP (10 μM) for 4 h. Cells were further fixed for 12 h with 4% paraformaldehyde (PFA) and blocked with 1% BSA and 0.3% Triton X-100 in PBS for 30 min. Then, rabbit anti-H3Cit and mouse anti-MPO primary antibodies were used overnight at 4 °C. After three washes, Alexa Fluor 488 donkey anti-rabbit IgG and Alexa Fluor Cy3 donkey anti-mouse IgG were added for 1.5 h at room temperature. Neutrophil-derived NET formation was visualized by fluorescence microscopy (LEICA DM2500).

Scanning electron microscopy

After isolating mouse neutrophils from bone marrow, neutrophils were stimulated with LPS, L-OHP, and L-OHP + LPS and incubated on a 22 × 22 mm cover glass for 4 h at 37 °C in a 5% CO2 incubator. Then, the cells were fixed with 2.5% glutaraldehyde for 30 min, dehydrated with 25%, 50%, 75% and 100% ethanol for 10 min each time, critical-point dried and then coated with 2 nm platinum. Since the NETs are fragile, each step was done with minimal disturbance of the media to preserve the structures. After dehydration and critical point drying, the specimens were analysed under a scanning electron microscope (Helios G4 CX, Thermo Scientific).

Immunohistochemistry

After mice were euthanized, hind paws were severed near the tarsal bones and prepared for histology using routine techniques after decalcification. Briefly, the sections were deparaffinized, rehydrated, and immersed in 3% hydrogen peroxide in methanol to quench endogenous peroxidase activity. And then the sections were incubated with blocking buffer for 1 h. The cross-sections of hind paws were stained with anti-H3Cit or anti-CD31 overnight at 4 °C. Staining was visualized by LEICA DM2500 microscopy. For each animal, three fields from cross-sections of the hind paw were visualized under ×20 and ×40 objectives. Three images from each animal were analyzed using ImageJ software. Intensity measurements were assessed by setting a "threshold" using the thresholding tool of ImageJ. The information on antibodies applied in this study referred to Reagent Validation.

Quantification of cell free DNA

Peripheral blood samples from cancer patients with/without chemotherapy (chemotherapy regimen containing oxaliplatin) and healthy donors were provided by Nanjing First Hospital. The sample collection processes followed approved institutional review board protocols with patients providing informed consent. Whole blood samples were drawn in an 8.5 mL heparin tube, and plasma was collected by centrifugation at 3000 r for 5 min. cf-DNA in plasma was quantified according to the manufacturer's instructions using the Quant-iT PicoGreen dsDNA Assay kit (P11496, Invitrogen).

Quantification of NETs

Mice plasma and human plasma were collected from whole blood by centrifugation at 3000 rpm for 5 min. NETs in plasma were quantified according to the manufacturer's instructions with the Citrullinated Histone H3 ELISA Kit (501620, Cayman), NETosis Assay Kit (601010, Cayman) and Quant-iT PicoGreen dsDNA Assay kit (P11496, Invitrogen). The absorbance was measured by microplate reader (Multiskan FC, ThermoFisher).

Measurement of DRG ROS

After digesting the DRG with 0.25% trypsin, the cell suspension was collected and screened with a 70 μm cell

strainer. Then, cell debris was removed by low-speed centrifugation. The cell supernatant was added to 2 ml PBS and mixed thoroughly, and then ROS were measured by DCFH-DA (S0033S, Beyotime) as a fluorescence probe. When DCFH formed inside cells, it was oxidized by intracellular ROS and converted to DCF; therefore, the detected fluorescence signal was proportional to ROS production.

Western blot

DRG samples were collected and washed with ice-cold PBS and then lysed in radioimmunoprecipitation assay (RIPA) buffer [Beyotime, Shanghai, China; 50 mM Tris (pH 7.4), 150 mM NaCl, 1% Triton X-100, 1% sodium deoxycholate, 0.1% sodium dodecyl sulfate, 1 mM phenylmethylsulfonyl fluoride, 0.15 U/mL aprotinin, and 1 mg/mL pepstatin]. Sample lysates were separated by SDS–PAGE and electrophoretically transferred onto polyvinylidene fluoride membranes. The membranes were blocked with 10% whole milk in TBST (Tris–HCl, NaCl, Tween 20) for 2 h at room temperature and probed with primary antibody at 4 °C overnight. The dilution factors of primary antibodies were neutrophil elastase (NE), H3Cit, H3, TF, HIF-1α and β-actin. Then, the membranes were incubated with horseradish peroxidase-coupled secondary antibodies from Sigma. Data were acquired with a Molecular Imager (Chem-iDoc, Bio–Rad) and analysed with ImageJ (Rawak Software). The information on antibodies applied in this study referred to Reagent Validation.

Statistical analysis

Prism 7.0 (GraphPad) was used to conduct all statistical analyses. Data were statistically evaluated by one-way or two-way ANOVA with Tukey's test. The results are presented as the mean ± standard error of three independent experiments. The results described as significant were based on a criterion of $P < 0.05$.

Role of funders

The funders did not have any role in study design, data collection, data analyses, interpretation or writing of the report.

Results

Chemotherapy induces NETs formation

To determine whether chemotherapy could drive NETs formation, we exposed mice to L-OHP for five consecutive days to induce CIPN. L-OHP-induced mechanical hyperalgesia was assessed by the Von Frey filaments test. L-OHP-treated animals exhibited significant mechanical touch-induced pain from day 3 to day 14 due to neurological toxicity, as shown in Fig. 1a. Subsequently, we examined the level of NE in plasma as a marker of NETs[10] at days 2, 7 and 14 after L-OHP administration. As shown in Fig. 1b, NE was significantly higher in the L-OHP-treated group than in the saline-treated group. This result suggested that chemotherapy induced neutrophils to form extracellular traps. To further investigate NETs formation induced by L-OHP, we examined the concentration of circulating free DNA (cf-DNA), which represents the remnants of NETs in plasma.[11,12] We found that the level of cf-DNA was higher in L-OHP-treated mice than in saline-treated mice (Fig. 1c). Moreover, we also investigated the effect of two other platinum analogs, carboplatin (CBP) and cisplatin (DDP), on inducing NETs formation. As shown in Fig. 1c, CBP and DDP increased the concentration of cf-DNA in the serum of mice compared with the saline-treated group. The ability of DDP to induce NETs formation is higher than that of the other twoTo further investigate NETs formation induced by L-OHP, we examined neutrophils in the blood of mice at 12 h, 24 h and 48 h after chemotherapy (L-OHP, 3 mg/kg, i.p.). $CD45^+$, $CD11b^+$ and $Ly\text{-}6G^+$ cells are presumably neutrophils. As shown in Fig. 1d and 12 h after chemotherapy, neutrophils in blood were significantly higher than those at 0 h. It reached a peak value and then declined after 24 and 48 h. Infection or tissue damage could stimulate the release of GM-CSF to increase the lifespan of neutrophils,[13] and this amplified neutrophil population provides defense against invading pathogens. Neutrophils may enter suicidal cell death to form NETs. Therefore, we speculated that the rapid increase and subsequent decline in neutrophils were probably caused by NETs formation. In addition, immunoblot data indicated that the levels of citrullinated histone H3 (H3Cit) and NE in the DRG were higher in the L-OHP-treated group than in the control group (Fig. 1e). H3Cit ELISA kit also showed that the levels of H3Cit in the plasma were higher in the L-OHP-treated group than in the control group (Fig. 1f). Moreover, we found a marked increase in the total content of the neutrophil enzyme MPO in the DRG after L-OHP treatment (Supplementary Fig. S2). Next, we investigated whether NETs form during chemotherapy by pathological assessment. We sought to determine whether NETs emerge in the paws of mice that are always influenced by chemotherapy after L-OHP administration. Immunohistochemistry staining of cross sections showed that H3Cit was abundant in the dermis and subcutaneous tissue where sensory neurons were distributed (Fig. 1g). In addition, H3Cit was also abundant in arteries. The immunohistochemistry staining of CD31 showed the location of arteries (Fig. 1h). Moreover, as shown in Fig. 1i, we detected robust NETs formation in the DRGs of mice. As typical NETs markers, MPO and NE emerged after L-OHP administration. Furthermore, we also detected that MPO and NE colocalized with CD31 (endothelial cell marker). We performed immunofluorescence experiment and immunohistochemistry experiment with isotype antibody and provided the staining control images in the Supplementary Fig. S3 to prove the specific stain. These results suggested that NETs formed in blood vessels and may cause microcirculation disturbance.

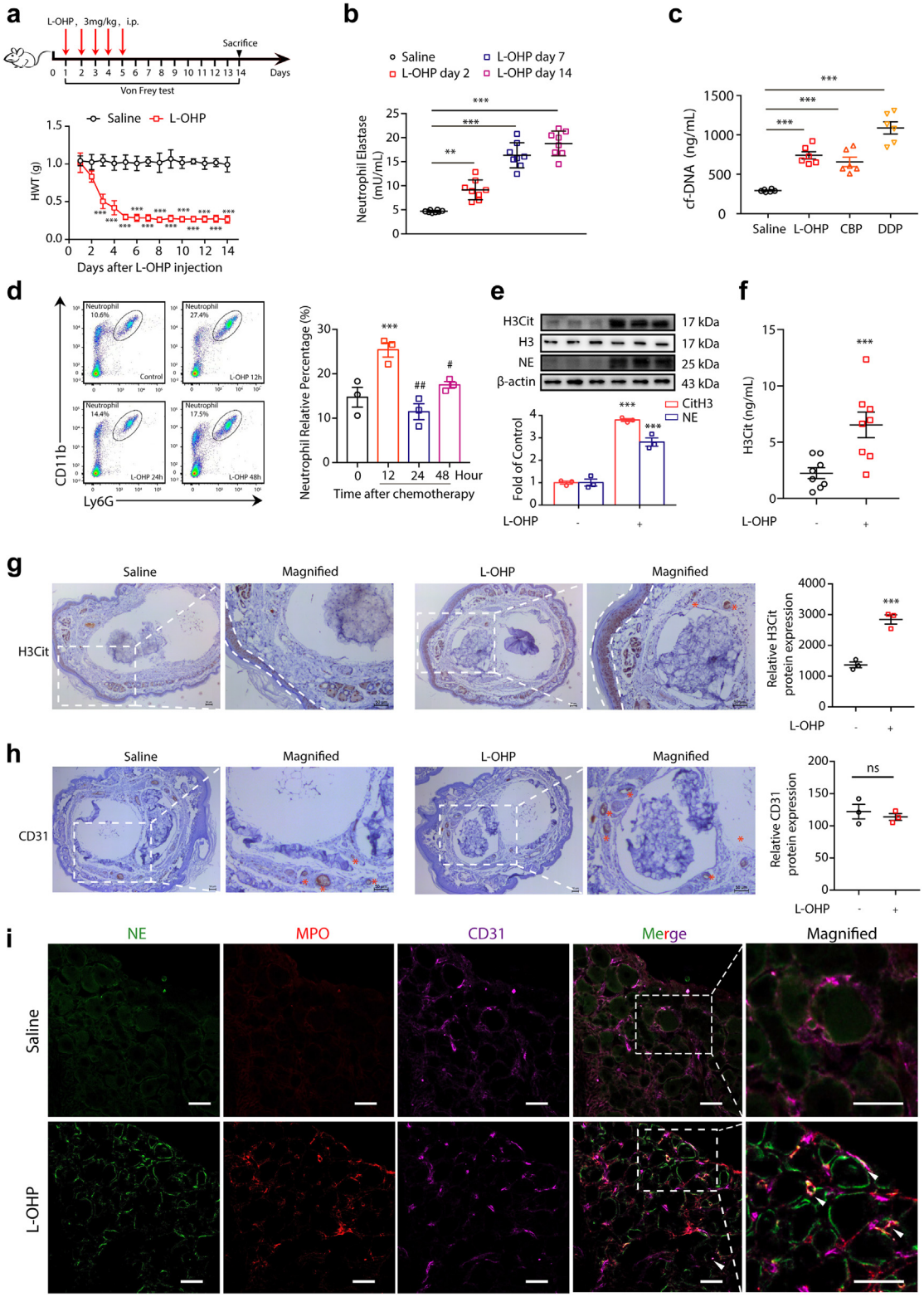

Fig. 1: **Chemotherapy triggers NETs formation. (a)** Mice were intraperitoneally injected with L-OHP (3 mg/kg) for five consecutive days to induce mechanical hyperalgesia. The mechanical pain threshold was tested for 14 days by Von Frey Hairs. Significant differences were revealed

Finally, we further validated our data by utilizing plasma samples from human participants (Supplementary Tables S1 and S2). As shown in Fig. 2a and b, the levels of H3Cit and cf-DNA in plasma from cancer participants who received chemotherapy were higher than that of healthy participants and higher than that of cancer participants who did not receive chemotherapy. This implies that NETs may play a critical role in the development of CIPN. To further explore the relationship between NETs formation and chemotherapy, Spearman correlation analysis was performed. The results indicated that there was a positive correlation between the total dose of L-OHP and H3Cit ($r = 0.8282$, $P < 0.001$; Fig. 2c). Furthermore, Spearman analysis suggested that there was a correlation between H3Cit and VAS scores. Correlation analysis revealed a correlation coefficient of $r = 0.8134$ ($P = 0.002$; Fig. 2d), indicating a positive correlation between the dose of NETs formation and chemotherapy-induced peripheral neuropathy. Similarly, there was a strong correlation between the total dose of L-OHP and VAS ($r = 0.8681$, $P < 0.0001$; Fig. 2e).

Disruption of NETs prevents chemotherapy-induced hyperalgesia by improving peripheral microcirculation disturbance

To investigate whether NETs are crucial to the development of CIPN, we utilized DNase1[14] to degrade L-OHP-induced NETs in a CIPN animal model. Compared with the L-OHP-treated group, DNase1 significantly reduced the elevated concentration of NE induced by L-OHP in the plasma of mice (Fig. 3a). It also decreased the levels of H3Cit and NE in the DRG compared with the L-OHP-treated group (Fig. 3b). To further confirm the effect of DNase1 on L-OHP-induced NETs, an immunofluorescence assay was employed in the DRGs. We observed that NETs were sufficiently degraded by DNase1 (Fig. 3c). Finally, we found that DNase1 treatment effectively improved the reduction in the baseline nociceptive threshold caused by L-OHP (Fig. 3d). Moreover, we started to treat mice with DNase1 after L-OHP administration, and we found that DNase1 treatment partially improved the reduction of baseline nociceptive threshold, which is not as good as concomitant administration of DNase1 together with L-OHP (Supplementary Fig. S4).

The characteristics of CIPN are the symptoms affecting both the lower and upper extremities in a "glove and stocking" distribution.[15] To mechanistically reveal the role of NETs in the development of CIPN, we utilized a laser Doppler speckle flowmeter to detect the dynamic changes in blood flow in the extremities of mice. As shown in Fig. 3e, after L-OHP treatment, the average value of blood flow in the lower limbs of mice was significantly reduced compared with the control group, while DNase1 could significantly improve the blood flow of the lower limbs compared with the L-OHP-treated groups. These data suggested that NETs may lead to microcirculatory disturbances.

It was reported that a stroke-homing peptide (SHp, CLEVSRKNC) could be recruited to the ischemic site of the body.[16,17] For active drug delivery in the treatment of ischemic stroke, SHp was identified and optimized by in vivo phage display in a focal cerebral ischemia rat model. SHp selectively targets the ischemic site in the brain and colocalizes to a portion of neuronal cells undergoing apoptosis in the penumbra region of ischemic brain tissue.[17] Similarly, to further evaluate the ischemic status caused by NETs, Cy5-SHp was delivered into the circulatory system of mice by tail vein injection (1 mg per mouse). The ischemic status of the limbs and sciatic nerve in vivo was observed using visible light imaging technology. As shown in Fig. 3f and g, ischemic conditions of the extremities and sciatic nerve were detected after L-OHP administration, while DNase1 significantly improved the ischemic condition. To further confirm the ischemic status of the limbs and sciatic nerve caused by L-OHP, we also investigated the corresponding biomarkers by Western blot. As shown in Fig. 3h, L-OHP elevated the level of hypoxia-inducible factor (HIF-1α) in the DRG, while DNase1 inhibited the upregulation of HIF-1α caused by L-OHP. It was reported that NETs-

following one-way ANOVA (n = 8, $^{***}P < 0.001$ *vs.* saline). Hindpaw mechanical withdrawal threshold (HWT) was examined at indicated time points after oxaliplatin therapy. **(b)** After intraperitoneal injection of L-OHP (3 mg/kg), the content of NETs in blood after 2, 7, and 14 days was evaluated by a NETosis Assay Kit. **(c)** After intraperitoneal injection of L-OHP (3 mg/kg) for 5 days, CBP (10 mg/kg) for 1, 3, and 7 days, and DDP (2.3 mg/kg) for 5 days, the content of cf-NDA in blood was evaluated by a Quant-iTPico green dsDNA kit. CBP= Carboplatin, DDP = Cisplatin. B and C Data were analysed by one-sample t test ($^{***}P < 0.001$ *vs.* saline). **(d)** 12, 24, and 48 h after a single intraperitoneal injection of L-OHP (3 mg/kg), the proportion of neutrophils in the peripheral blood of mice was evaluated by flow cytometry, and the neutrophils were labeled with triple positivity of CD45, CD11b, and Ly-6G. Data were analysed by one-way ANOVA (n = 3, $^{***}P < 0.001$ *vs.* 0 h; $^{\#}P < 0.05$, $^{\#\#}P < 0.01$ *vs.* 12 h). **(e)** The protein levels of H3Cit and NE in the DRG were evaluated on the 14th day by Western blot. Data were analysed by one-way ANOVA (n = 3, $^{***}P < 0.001$ *vs.* saline). **(f)** The levels of H3Cit in the plasma were evaluated on the 14th day by H3Cit ELISA kit. Data were analyzed by one-sample t test ($^{***}P < 0.001$ vs. saline). **(g)** Representative microscopy images of hind paw cross-sections from mice treated with saline or L-OHP and stained with the NETs marker H3Cit. The zones of the dermis and subcutaneous tissue are labeled with dotted lines, and the arteries are labeled with asterisks. Scale bars, 50 μm. **(h)** Representative microscopy images of hind paw cross-sections from mice treated with saline or L-OHP and stained with CD31. Vessels were labeled with asterisks. Scale bars, 50 μm. **(i)** Representative confocal immunofluorescence microscopy images of DRG from mice treated with saline or L-OHP for 14 days and stained with NE (green), MPO (red) and CD31 (purple); arrowheads point to NETs in vessels. Scale bars, 50 μm.

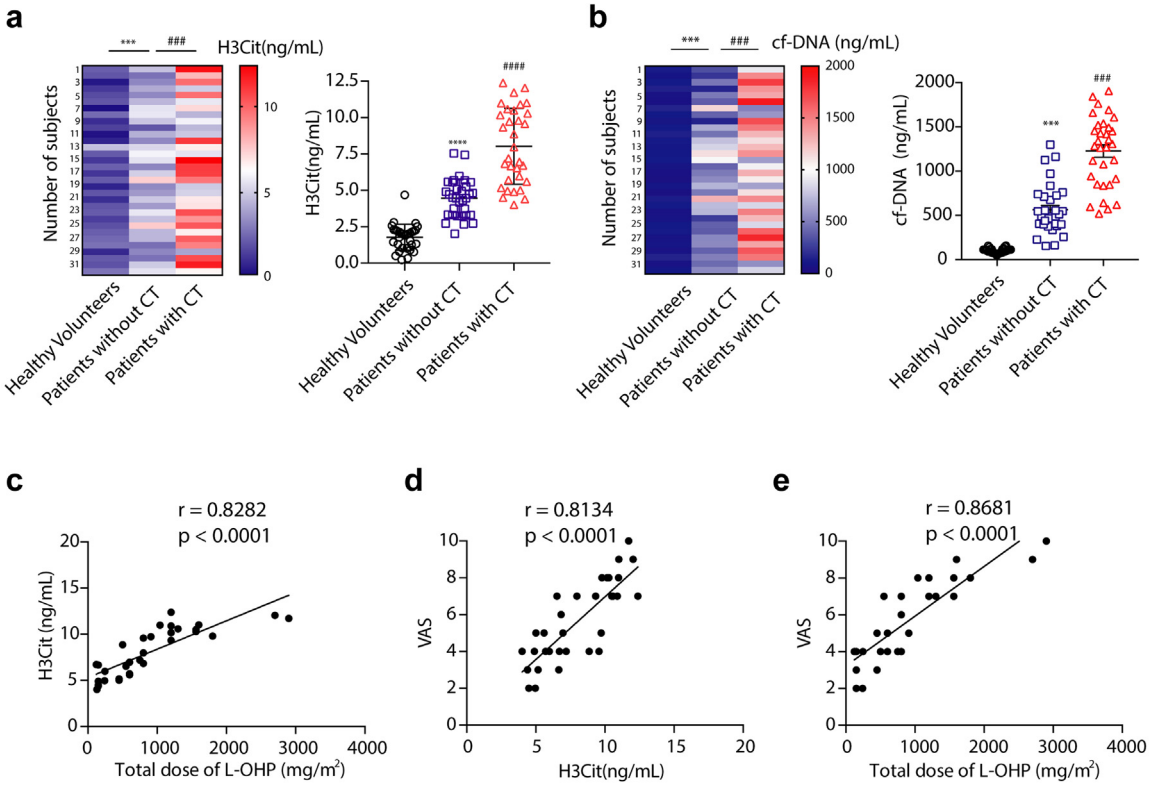

Fig. 2: **NETs presents in the plasma of patients after chemotherapy. (a** and **b)** The level of H3Cit and cf-DNA measured by H3Cit ELISA kit and Quant-iTPico green dsDNA assay in plasma from healthy volunteers and cancer patients who had or had not received chemotherapy (n = 10) Data was analysed by one-way ANOVA (n = 32 volunteers in each group; $^{***}P < 0.001$ *vs.* healthy volunteers; $^{\#\#\#}P < 0.001$ *vs.* patients without chemotherapy). **(c)** Correlation between H3Cit and the total dose of L-OHP were analyzed by linear regression analysis (n = 32 cancer patients receiving chemotherapy, $r = 0.8282$, $P < 0.0001$, linear regression analysis). **(d)** Correlation between VAS and H3Cit and the correlation in cancer patients after chemotherapy were analysed by linear regression analysis (n = 32 cancer patients with chemotherapy, $r = 0.8134$, $P = 0.0020$, linear regression analysis). **(e)** Correlation between VAS and total dose of L-OHP (n = 32 cancer patients receiving chemotherapy, $r = 0.8681$, $P < 0.0001$, linear regression analysis). cf-DNA = circulating free DNA; VAS = visual analogue scale.

bound NE could cleave tissue factor pathway inhibitors (TFPIs) to initiate thrombosis.[18] Therefore, we investigated the level of TF under L-OHP administration with or without DNase1 therapy. Western blot data indicated that DNase1 could inhibit the upregulation of TF caused by L-OHP (Fig. 3h). As a downstream effector of HIF-1α, an increase in MMP-9/2 activity is critical for the development of CIPN.[7] We investigated the effects of DNase1 on MMP-9/2 under L-OHP treatment. As shown in Fig. 3i, DNase1 reduced the elevated MMP-9/2 activity in chemotherapy-treated mice. Our results mentioned above fully demonstrated that the microcirculation disorder caused by NETs is a key factor in the generation of chemotherapy-induced hyperalgesia.

Gut microbiota is critical for L-OHP-induced NETs formation

L-OHP treatment could change the gut microbiota and destroy the gut epithelial barrier to permit LPS, a wall component of gram-negative bacteria, to enter the circulatory system.[19] Hematoxylin and eosin (H&E) staining data indicated intestinal pathologic changes in mice receiving L-OHP. As shown in Fig. 4a, the colon from control mice was intact; in contrast, L-OHP-treated mice exhibited a disrupted gut epithelial barrier and increased inflammatory infiltration. Compared with the control group, intestinal mucosal necrosis, disorderly cell arrangement, and intestinal mucosal thinning occurred in the intestines of mice receiving L-OHP on the 1st day, the injury worsened on the 3rd and 5th day, and the trend of inflammatory infiltration was similar. However, mice exposed to a cocktail of antibiotics in drinking water (free drinking daily for three consecutive weeks containing 0.5 g/L ampicillin, 0.5 g/L neomycin, 0.5 g/L metronidazole, 0.25 g/L vancomycin, and 3 g/L artificial sweetener Splenda) (abx mice) did not exhibit colonic structural damage or inflammatory infiltration in the colon after 5 days of L-OHP administration.

To further confirm intestinal barrier damage, we investigated the LPS content, a gram-negative bacterial

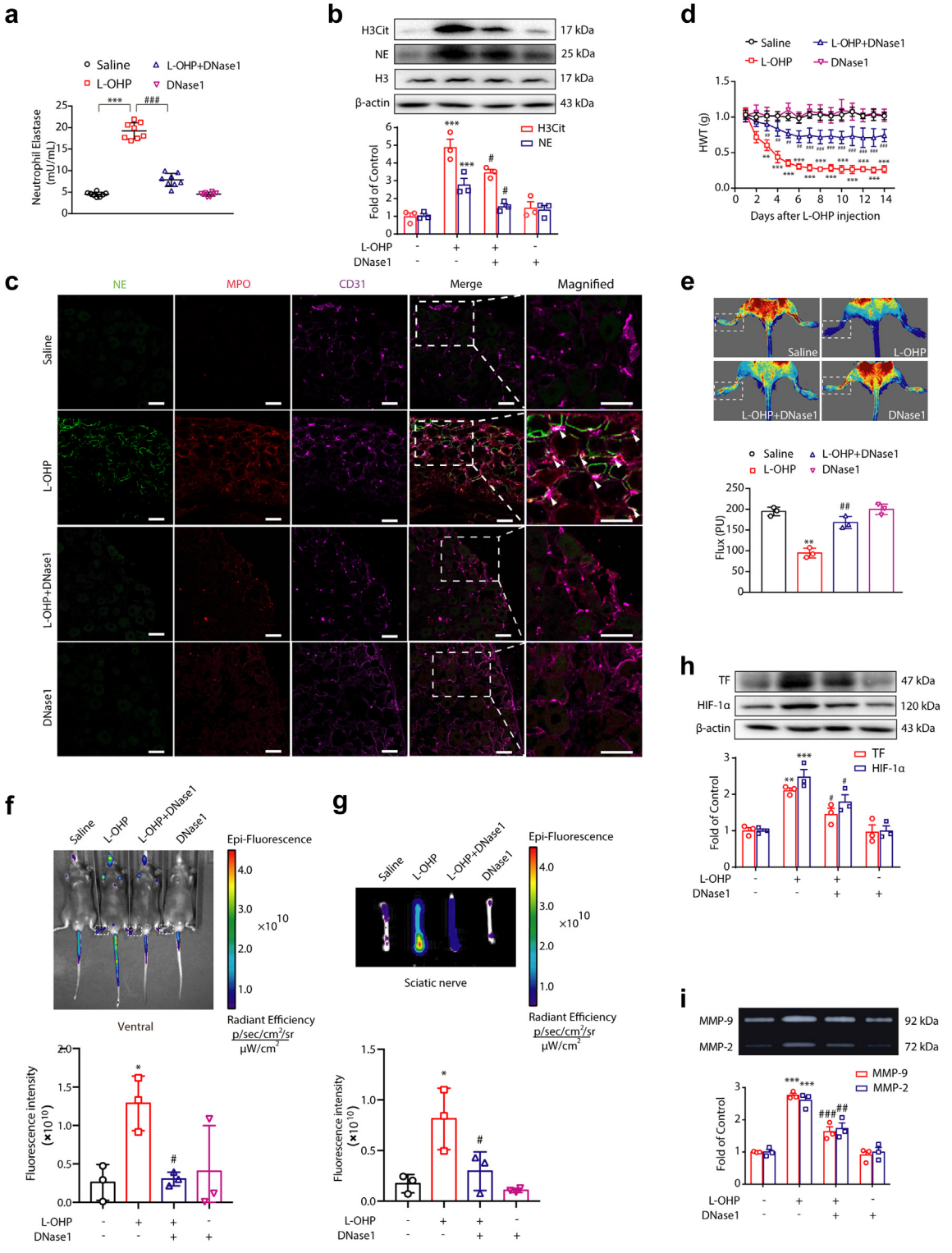

***Fig. 3:* DNase1 alleviates CIPN by degrading NETs.** Mice were intraperitoneally injected with L-OHP (3 mg/kg) for five consecutive days to induce mechanical hyperalgesia. DNase1 (150 U, i.v.) was administered from the first day of modeling to the 14th day. **(a)** The level of NETs in plasma was measured on the 14th day by a NETosis Assay Kit (n = 8). **(b)** The protein levels of H3Cit and NE in the DRG were evaluated on the 14th day by Western blot (n = 3). **(c)** Representative confocal immunofluorescence microscopy images of DRG from mice stained with NE

wall component, in the serum and DRG of chemotherapeutic mice. As shown in Fig. 4b and c, the levels of LPS in the serum and DRG of mice significantly increased after chemotherapy, while antibiotic administration decreased the LPS content compared with the L-OHP group. Furthermore, we measured the levels of IL-6 and TNF-α, cytokines associated with LPS-TLR4 signaling.[19] L-OHP administration markedly increased the levels of IL-6 and TNF-α in plasma and DRG (Supplementary Fig. S5), while the levels of IL-6 and TNF-α in the antibiotic-treated group were downregulated. This demonstrated that chemotherapy induced intestinal bacteria to enter the blood and triggered inflammation. LPS is a potent NETs trigger.[20] Therefore, we detected the content of NETs in the plasma of abx mice compared to L-OHP-treated mice. Surprisingly, as shown in Fig. 4d, antibiotics reduced the level of NETs in the plasma of chemotherapeutic mice. Then, we measured the mechanical pain threshold of the mice. As shown in Fig. 4e, the baseline nociceptive threshold declined significantly compared with the control group after L-OHP therapy and remained at a very low level for 14 days, while antibiotics could effectively relieve mechanical hyperalgesia in chemotherapeutic mice. Our data implied that gut-derived bacteria probably played a critical role in L-OHP-induced NETs formation. To further confirm the relationship between chemotherapy and NETs formation, we utilized primary neutrophils to investigate the effect of L-OHP on the generation of NETs. We stimulated neutrophils with L-OHP in the presence or absence of LPS. As shown in Fig. 4f, NETs were examined by scanning electron microscopy. L-OHP (10 μM) or LPS (10 ng/mL) did not trigger NETs formation. However, in the presence of LPS (10 ng/mL), L-OHP (10 μM) robustly induced NETs formation, which was similar to that induced by a high concentration of LPS (1 μg/mL, positive control).

Furthermore, as shown in Supplementary Fig. S6a, we found that L-OHP could cause an ROS burst in the DRG, which was consistent with previous studies.[19] It was reported that NETs formation depended on ROS. Therefore, we utilized N-acetylcysteine (NAC), a commonly used reagent against ROS,[21] to investigate the underlying mechanism in L-OHP-induced NETs formation. As shown in Supplementary Fig. S6b and c, NAC sufficiently decreased the level of cf-DNA in plasma and effectively relieved mechanical hyperalgesia in chemotherapeutic mice. Moreover, we isolated primary neutrophils from mice and found that NET formation induced by L-OHP with LPS could be blocked with the TLR4 inhibitor TAK242 or NAC and that TAK242 plus NAC could more effectively inhibit NETs formation (Supplementary Fig. S6d).

MPO and PAD4 are responsible for L-OHP-induced NETs formation

Bacteria-induced NETs formation can be mediated by MPO, NE or PAD4.[22–24] It was reported that these pathways mainly lie downstream of ROS signaling.[22,25] Therefore, we tested whether MPO was crucial for L-OHP-induced NETs formation. ELISA and Western blot data revealed that PF-1355 (50 mg/kg, i.p.), an MPO inhibitor, could sufficiently inhibit L-OHP-induced NET formation. It decreased the level of NE in plasma and the levels of H3Cit and NE in the DRG compared with the L-OHP-treated group (Fig. 5a and b). As shown in Fig. 5c, the baseline nociceptive threshold declined significantly compared with that of the control group after L-OHP therapy and remained at a very low level for 14 days, while PF-1355 effectively relieved mechanical hyperalgesia in chemotherapeutic mice. To investigate the circulatory state of extremities, we utilized a laser Doppler speckle flowmeter to detect the blood flow of mice, and we found that the average value of blood flow in the lower limbs of mice was significantly improved by PF-1355 compared with the L-OHP-treated group (Fig. 5d). In addition, the ischemic status of the lower limbs and sciatic nerve caused by L-OHP was alleviated by PF-1355 (Fig. 5e and f). Furthermore, as shown in Fig. 5g, PF-1355 inhibited the upregulation of HIF-1α caused by L-OHP. Inhibition of MPO also suppressed the L-OHP-induced upregulation of TF and the activities of MMP9/2 (Fig. 5g and h).

Another important pathway controlling NETs formation is PAD4-driven chromatin modification, which causes histone citrullination. It was reported that ROS are sufficient to activate PAD4.[24] Therefore, we investigated the role of PAD4 in L-OHP-induced NETs formation. We compared wildtype (WT) with PAD4-deficient ($Pad4^{-/-}$) mice or treated mice with a pan-PAD inhibitor Cl-amidine. There was a significant difference in the level of NE in plasma and the levels of H3Cit and NE in the DRG between WT and $Pad4^{-/-}$

(green), MPO (red) and CD31 (purple); arrowheads point to NETs in vessels (n = 3). Scale bars, 50 μm. **(d)** The mechanical pain threshold was tested for 14 days by Von Frey Hairs (n = 8). **(e)** Blood flow in the lower limbs of mice was evaluated by a moorFLPI2 flow speckle hemodynamic meter on the 14th day (n = 3). **(f** and **g)** SHp conjugated with the fluorescent dye Cy5-NHS was injected into mice via the tail vein. The ischemic condition of the limbs (f) and sciatic nerves (g) was evaluated by the IVIS Spectrum small animal in vivo visible three-dimensional imaging system after 2 h of SHp-Cy5 injection on the 14th day (n = 3). **(h)** The protein levels of TF and HIF-1α (n = 3) in the DRG were evaluated by Western blot. **(i)** The activities of MMP-9 (n = 3) in the DRG were evaluated by gelatin zymography. a, b, e, h and i data were analysed by one-way ANOVA. d data was analysed by two-way ANOVA. $^{**}P < 0.01$, $^{***}P < 0.001$ vs. saline; $^{\#}P < 0.05$, $^{\#\#}P < 0.01$, $^{\#\#\#}P < 0.001$ *vs. the* L-OHP-treated group.

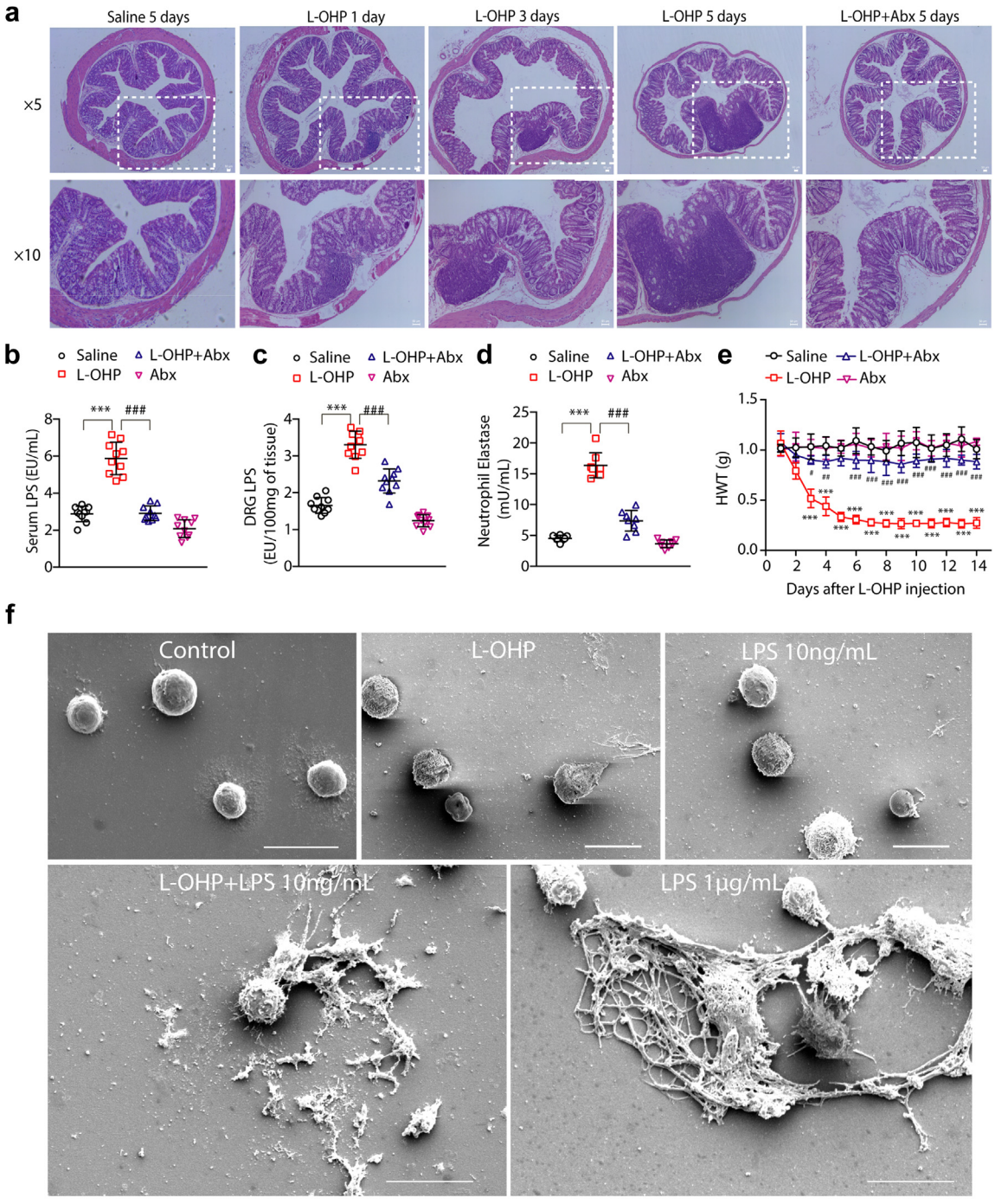

Fig. 4: **Chemotherapy induced gut microbe-derived NETs formation.** Mice were intraperitoneally injected with L-OHP (3 mg/kg) for 5 days, and antibiotics were added into the water three weeks in advance, which was freely ingested by the mice. **(a)** The degree of intestinal barrier and inflammatory infiltration was evaluated by H&E staining (n = 3). Scale bar, 50 μm. **(b** and **c)** LPS levels in the serum of mice were evaluated by a Pierce Chromogenic Endotoxin Quant Kit (n = 10). **(d)** The content of NETs in blood plasma was evaluated by a NETosis Assay Kit (n = 8). **(e)** The mechanical pain threshold was tested for 14 days by Von Frey Hairs (n = 8). **(f)** NETs formation was examined by scanning electron microscopy following stimulation of neutrophils with LPS (10 ng/mL), L-OHP (10 μM), LPS (10 ng/mL) + L-OHP (10 μM) for 4 h. Cells treated with LPS (1 μg/mL) were used as a positive control (n = 3). Scale bar, 10 μm. b–d data were analysed by one-way ANOVA. e data was analysed by two-way ANOVA. $^{***}P < 0.001$ *vs.* saline; $^{\#}P < 0.05$, $^{\#\#}P < 0.01$, $^{\#\#\#}P < 0.001$ *vs.* the L-OHP-treated group.

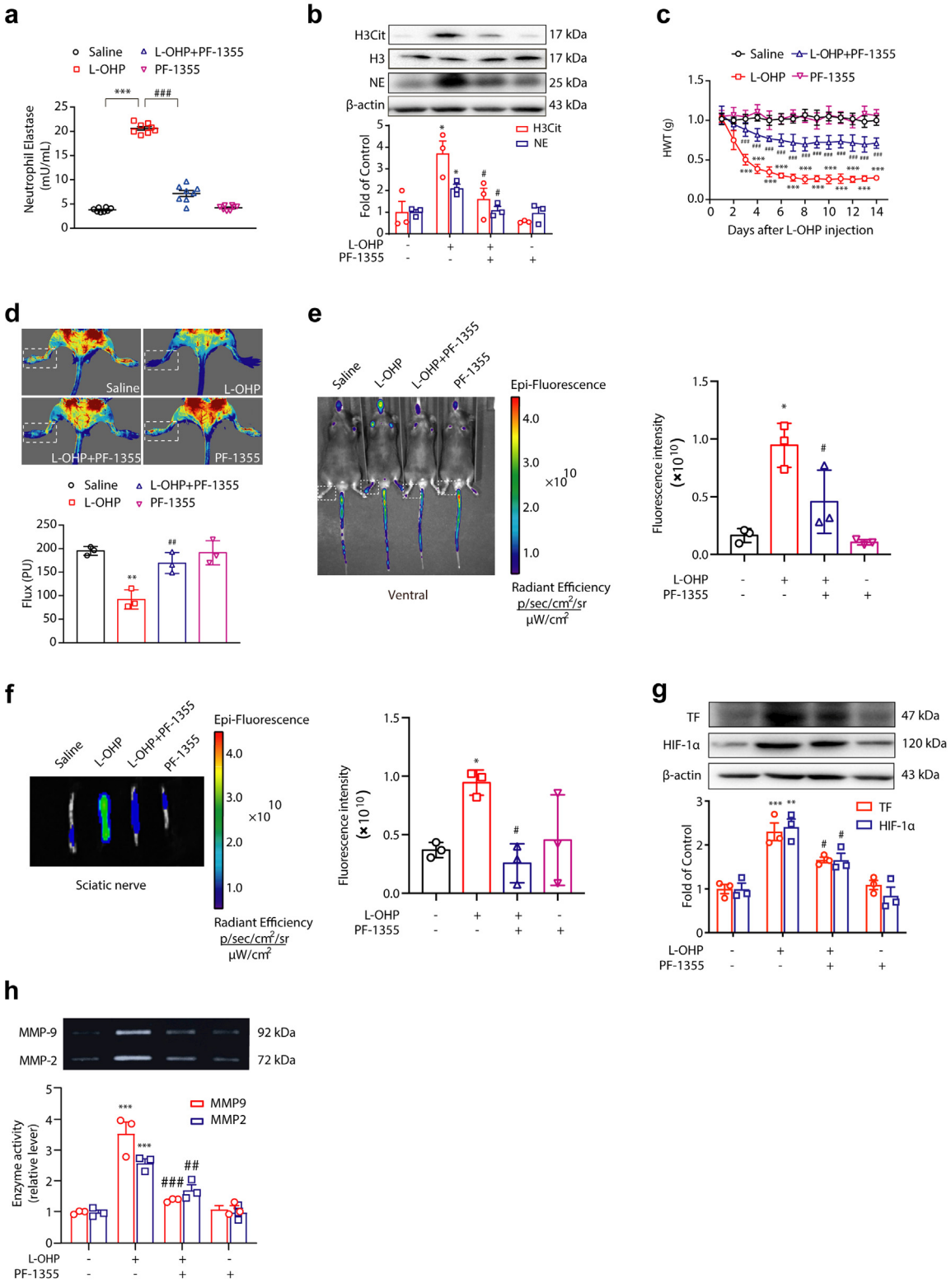

Fig. 5: **MPO is responsible for L-OHP-induced NETs formation.** Mice were intraperitoneally injected with L-OHP (3 mg/kg) for 5 days. MPO inhibitor PF-1355 (50 mg/kg, i.p.) was administered one day before L-OHP administration until the end of 14 days. **(a)** The levels of NETs in

mice (Fig. 6a and b). This kind of difference also occurred between the mice treated with or without Cl-amidine (Fig. 6c and d). Thus, these data provide evidence that PAD4 is responsible for NETs formation induced by L-OHP. The inhibition of PAD4 by genetic ablation or pharmacologic suppression dramatically improved chemotherapy-induced mechanical hyperalgesia (Fig. 6e and f). To further confirm the effects of PAD4 on L-OHP-induced NETs formation, triple immunofluorescence with confocal microscopy was performed on DRG sections. This analysis revealed that MPO and NE colocalized with the endothelial cell marker CD31 after L-OHP treatment (Supplementary Fig. S7), which was consistent with the data mentioned above, and NETs were sufficiently inhibited by the PAD4 inhibitor. PAD4 inhibition also improved the blood flow in the lower limbs of mice compared with the L-OHP-treated group (Fig. 6g and h) and ameliorated the ischemic status of the lower limbs and sciatic nerve caused by L-OHP (Fig. 6i–l). Subsequently, PAD4 inhibition suppressed the L-OHP-induced upregulation of TF and the activities of MMP9/2 (Fig. 6m–p).

SHp-DNase1 treatment prevented chemotherapy-induced mechanical hyperalgesia

As the SHp-conjugated dye Cy5-NHS could be effectively recruited to loci of L-OHP-induced NETs, SHp-conjugated DNase1 was employed to evaluate its function in chemotherapy-induced hyperalgesia. The mice were injected with SHp-DNase1 (SHp-DNase1 mice) via the tail vein every day from days 1–14. As shown in Fig. 7a, SHp-DNase1 sufficiently improved the ischemic condition of the limbs and sciatic nerves in mice. The baseline nociceptive threshold of L-OHP-treated mice declined significantly and remained at a very low level for 14 days. While SHp-DNase1 mice did not show changes in the baseline nociceptive threshold, mechanical hyperalgesia was not detectable after L-OHP therapy (Fig. 7b). It is more effective than DNase1 in the treatment of chemotherapy-induced hyperalgesia. As shown in Fig. 7c, SHp-DNase1 obviously improved the lower limb blood flow of mice, and the effect was better than that of DNase1 alone.

The above data demonstrate that NETs are critical in the development of CIPN. However, a key consideration of putative antihyperalgesia treatments is their effect on tumor progression and chemotherapy. As oxaliplatin is commonly used for the treatment colon cancer, we thus sought to investigate the effect of Cl-amidine and DNase1 in MC38 cells induced mice tumor model. The results showed that PAD4 inhibitor and DNase1 did not affect tumor progression or chemotherapy efficacy (Supplementary Fig. S8).

Discussion

In this study, we show in a model of L-OHP-induced CIPN that the activation of NETs is critical in the development of microcirculation disturbance and peripheral neuropathies, and that interfering with NETs formation may be a useful strategy to alleviate chemotherapy-induced neurotoxicity. (1) The occurrence of CIPN is related to the generation of NETs. Chemotherapy results in intestinal inflammatory infiltration and gut epithelial barrier leak, and neutrophils are activated leading to the production of NETs and the occurrence of CIPN consequently. (2) With the process of chemotherapy, NETs accumulate continuously and causes the microcirculation disturbance in extremities, sciatic nerve and DRG, which results in ischemia and hypoxia and induces the expression of TF and HIF-1α with MMP-9/2 activation. (3) The inhibition of MPO or PAD4 by pharmacologic suppression or genetic ablation could sufficiently alleviate CIPN, correspondingly reducing the levels of TF, HIF-1α and the activities of MMP-9/2. DNase1 can sufficiently improve L-OHP-induced mechanical hyperalgesia by degrading NETs, especially SHp-DNase1, which contains ischemic homing peptide, can target the ischemic sites in extremities and peripheral nerves of mice more effectively.

As a common dose-limited effect of chemotherapy, CIPN not only compels patients to reduce the dosage of chemotherapeutic agents, but also causes anxiety and depression hindering the therapeutic effect and negatively impacting outcomes.[25,26] Previous studies showed that chemotherapy increased the protein levels of TF and HIF-1α, and a large number of clinical reports showed that cancer and chemotherapy greatly increase the risk of vascular occlusion.[27] The characteristics of CIPN is “glove and stocking” distribution in lower and upper extremities with severe pain. In our study, the blood flow of extremities was disrupted after chemotherapy. However, a high-efficiency anticoagulant hirudin only partially improved microcirculation effectively

plasma were evaluated on the 14th day by a NETosis Assay Kit (n = 8). **(b)** The protein levels of H3Cit and NE in the DRG were evaluated on the 14th day by Western blot (n = 3). **(c)** The mechanical pain threshold was tested for 14 days by Von Frey Hairs (n = 8). **(d)** Blood flow in the lower limbs of mice was evaluated by a moorFLPI2 flow speckle hemodynamic meter on the 14th day (n = 3). **(e** and **f)** SHp conjugated with the fluorescent dye Cy5-NHS was injected into mice via the tail vein. The ischemic condition of the limbs (e) and sciatic nerves (f) was evaluated by the IVIS Spectrum small animal in vivo visible three-dimensional imaging system after 2 h of SHp-Cy5 injection on the 14th day (n = 3). **(g)** The protein levels of TF and HIF-1α (n = 3) in the DRG were evaluated by Western blot. **(h)** The activities of MMP-9 (n = 3) in the DRG were evaluated by gelatin zymography. a, b, g and h data were analysed by one-way ANOVA. c data was analysed by two-way ANOVA. $^{*}P < 0.05$, $^{**}P < 0.01$, $^{***}P < 0.001$ *vs.* saline; $^{\#}P < 0.05$, $^{\#\#}P < 0.01$, $^{\#\#\#}P < 0.001$ *vs.* the L-OHP-treated group.

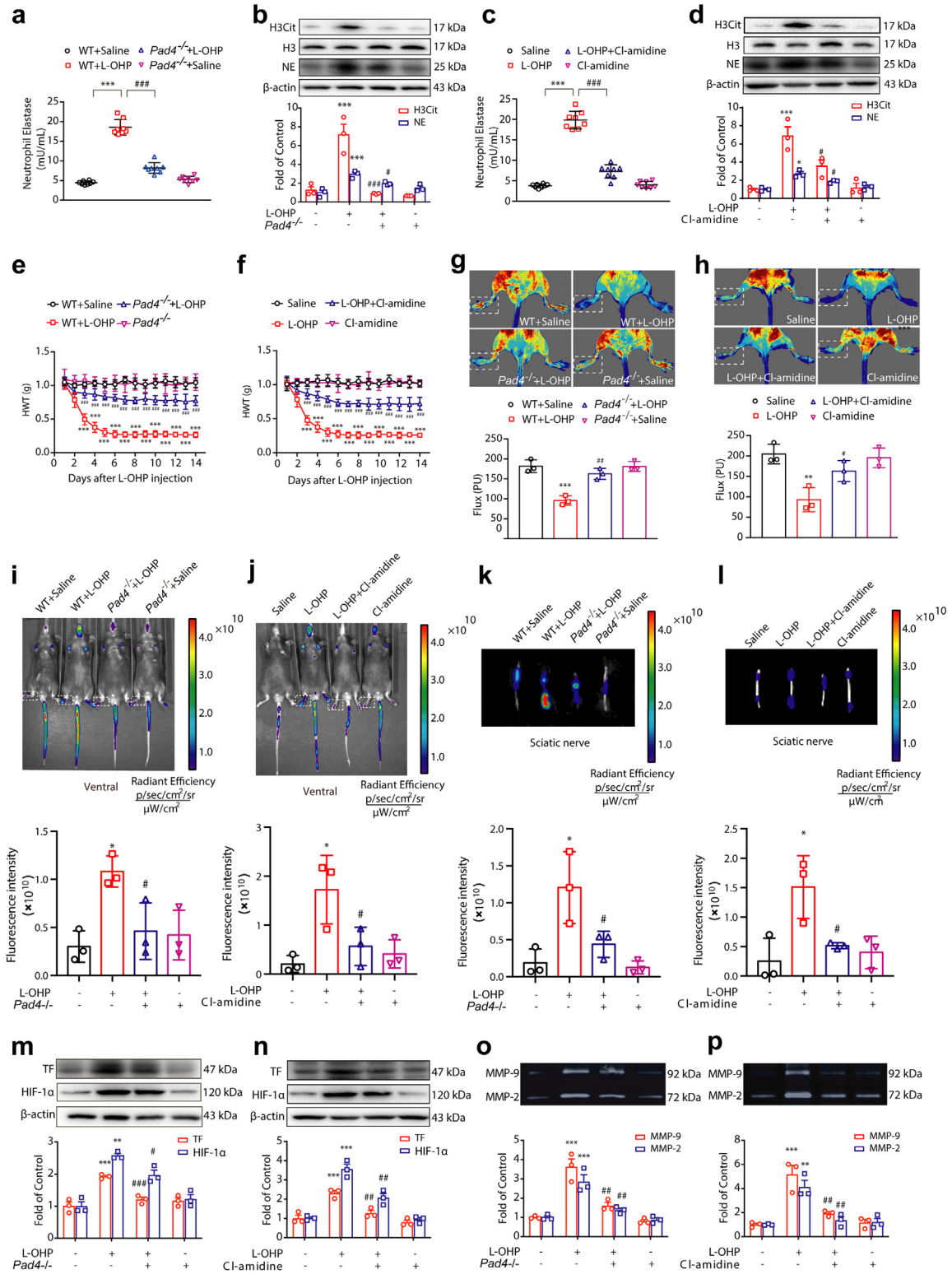

Fig. 6: **PAD4 is responsible for L-OHP-induced NETs formation.** Mice were intraperitoneally injected with L-OHP (3 mg/kg) for 5 days. *Pad4*$^{-/-}$ mice were used to investigate NETs formation induced by L-OHP. Cl-amidine (10 mg/kg, i.p.) was administered one day before L-OHP administration until the end of 14 days. **(a** and **c)** The levels of NETs in plasma were evaluated on the 14th day by a NETosis Assay Kit (n = 8).

(Supplementary Fig. S1) as well as the chemotherapy-induced hyperalgesia, this implied a noncanonical thrombosis occurred during CIPN. Therefore, we tried to figure out whether there was another mechanism that caused microcirculation disorder to explain the pathogenesis of CIPN. Previous researchers observed that NETs were frequently associated with ischemic organ damage.[28] Pathogen-derived stimulation could promote intravascular NETs forming clots that obstructed blood vessels and caused organ damage.[29] Oxaliplatin, a platinum-based chemotherapeutic agent, could evoke pathogen-derived stimuli and ROS which are the two critical factors in inducing NETs formation. The chemotherapy of cancer is often accompanied with infection resulting from neutropenia.[30] Therefore, we speculated that neutrophil and NETs might be involved in CIPN. Therefore, we investigated the level of neutrophils in blood of mice at 12 h, 24 h and 48 h after L-OHP single injection. The results showed that at 12 h after chemotherapy, neutrophils had a short burst of increase, and then dramatically decreased to low level (Fig. 1b). Why did the concentration of neutrophils in circulation decrease rapidly? As observed in tumor and thrombotic diseases, after being stimulated, neutrophils released their own mitochondrial and nuclear chromatin DNA to the outside encapsulating various granzymes to form a fibrous reticulum like structure named NETs, and then died and were cleaned by macrophages.[10] We detected the content of NETs in the blood from mice treated with L-OHP for 2, 7 and 14 days. The results showed that the level of NETs in blood significantly increased after L-OHP administration (Fig. 1c), indicating that neutrophils were activated to release NETs. At the same time, we detected NETs in the blood of patients with oxaliplatin and found that the level of NETs in plasma of patients with chemotherapy was significantly higher than that of patients without chemotherapy (Fig. 2a and b). However, it is unclear how the neutrophils were activated. Shen et al. reported that the gut microbes promoted the mechanical pain hypersensitivity of mice after chemotherapy.[19] Meanwhile, they found that the mechanical pain hypersensitivity induced by L-OHP was reduced in sterile mice and antibiotic-pretreated mice and the hyperalgesia was mediated by TLR4 on macrophages. Therefore, we examined the colonic intestinal pathology of mice within 5 days of chemotherapy and found that mice treated with L-OHP represented disrupted gut epithelial barrier and increased inflammation infiltration (Fig. 4a). Then we found that antibiotics reduced the NETs in blood (Fig. 4d) and antibiotics also reduced the mechanical pain threshold in L-OHP-treated mice (Fig. 4e).

The DRG is located between the dorsal root and the spinal nerve. It contains pseudounipolar neurons that convey sensory information from the periphery to the central nervous system.[31] Since hyper excitability of DRG neurons is proposed as an important component for neuropathic pain, more and more attention has been paid to the role of DRG in the pathogenesis of CIPN.[31] In accord with some recent findings,[19] our data further showed that LPS content in serum and DRG of mice increased significantly after L-OHP treatment (Fig. 4b and c). Chemotherapy-induced inflammation has been reported to be associated with dysregulation of colonic bacterial homeostasis in mice.[32] Behavioral changes, central and peripheral immune system activation, colonic tissue integrity, and simultaneous changes in bacterial community structure have been observed in paclitaxel-treated mice.[33] Chemotherapy led to increased fatigue and cognitive decline in mice, increased microglial immune reactivity, and severe colon damage. It also elevated expression of chemokines (CXCL1) in circulating blood and transient elevation of proinflammatory cytokines/chemokines (TNF-α, IL-6).[34] In this study, after 14 days chemotherapy, we found that L-OHP could indeed elevate the levels of TNFα and IL-6 in the blood and DRG from mice, while antibiotics could reduce the levels of these cytokines (Supplementary Fig. S5). Thus, neutrophil activation and NETs release may be due to the inflammatory environment represented by high concentration of LPS and inflammatory factors after chemotherapy.

NETs consist of extruded chromosomal DNA decorated with granular components including antimicrobial peptides and proteases.[35] A large number of studies showed that the mechanisms leading to the NETs formation included calcium mobilization, production of ROS, activation of MPO, and chromatin modification by PAD4 through histone citrullination.[24,36,37] Therefore, we used PF-1355 and Cl-amidine to investigate whether CIPN process is related to NETs. The levels of NE and H3Cit could be used as indicators for the detection of

(b and **d)** The protein levels of H3Cit and NE in the DRG were evaluated on the 14th day by Western blot (n = 3). **(e** and **f)** The mechanical pain threshold was tested for 14 days by Von Frey Hairs (n = 8). **(g** and **h)** Blood flow in the lower limbs of mice was evaluated by a moorFLPI2 flow speckle hemodynamic meter on the 14th day (n = 3). **(i–l)** SHp conjugated with the fluorescent dye Cy5-NHS was injected into mice via the tail vein. The ischemic conditions of the limbs (i and j) and sciatic nerves (k and l) were evaluated by the IVIS Spectrum small animal in vivo visible three-dimensional imaging system after 2 h of SHp-Cy5 injection on the 14th day (n = 3). **(m** and **n)** The protein levels of TF and HIF-1α (n = 3) in the DRG were evaluated by Western blot. **(o** and **p)** The activities of MMP-9 (n = 3) in the DRG were evaluated by gelatin zymography. a–d, g, h, m–p data were analysed by one-way ANOVA. e and f data were analysed by two-way ANOVA. $^{**}P < 0.01$, $^{***}P < 0.001$ *vs.* saline; $^{\#}P < 0.05$, $^{\#\#}P < 0.01$, $^{\#\#\#}P < 0.001$ *vs.* L-OHP-treated group in a, b, e, g, m and o data. $^{*}P < 0.05$, $^{**}P < 0.01$, $^{***}P < 0.001$ *vs.* saline; $^{\#}P < 0.05$, $^{\#\#}P < 0.01$, $^{\#\#\#}P < 0.001$ vs. WT + L-OHP group in c, d, f, h, n and p data.

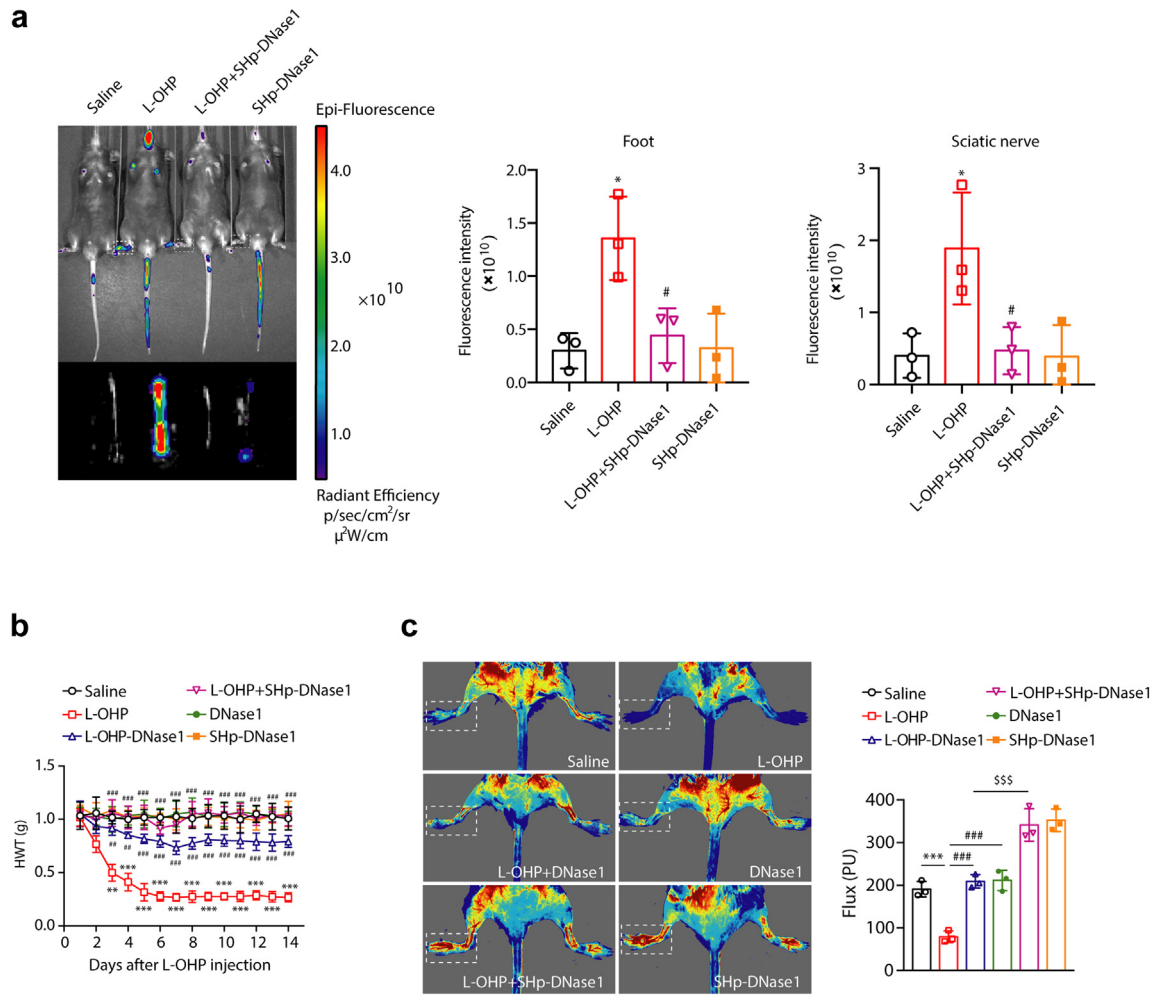

***Fig. 7:* SHp-DNase1 treatment prevents chemotherapy-induced mechanical hyperalgesia.** Mice were intraperitoneally injected with L-OHP (3 mg/kg) for five consecutive days to induce mechanical hyperalgesia. **(a)** SHp-Cy5 was injected into mice via the tail vein. The ischemic condition of the limbs and sciatic nerves was evaluated by the IVIS Spectrum small animal in vivo visible three-dimensional imaging system after 2 h of SHp-Cy5 injection on the 14th day (n = 3). **(b)** DNase1 (150U, i.v.) or SHp-DNase1 (150U, i.v.) was administered from the first day of modeling to the 14th day. The mechanical pain threshold was tested for 14 days by Von Frey Hairs (n = 8). Data were analysed by two-way ANOVA. $^{**}P < 0.01$, $^{***}P < 0.001$ *vs.* saline; $^{\#\#}P < 0.01$, $^{\#\#\#}P < 0.001$ *vs.* the L-OHP-treated group. **(c)** DNase1 (150U, i.v.) or SHp-DNase1 (150U, i.v.) was administered from the first day of modeling to the 14th day. Blood flow in the lower limbs of mice was evaluated by a moor FLPI2 flow speckle hemodynamic meter on the 14th day (n = 3). Data were analysed by one-way ANOVA. $^{***}P < 0.001$ *vs.* saline; $^{\#}P < 0.05$, $^{\#\#\#}P < 0.001$ *vs.* the L-OHP-treated group. $^{\$}P < 0.05$ vs. L-OHP-DNase1-treated group.

NETs.[10] After establishment of CIPN model, the NE level, which significantly increased in plasma of mice, could be effectively reduced by PF-1355 or Cl-amidine (Figs. 5a and 6c). The data of H3Cit were consistent with NE (Figs. 5b and 6d). Then we measured the mechanical pain threshold of mice. PF-1355 and Cl-amidine could both effectively prevent the chemotherapy-induced mechanical pain (Figs. 5c and 6f). Comparing with WT mice, the mechanical pain was also sufficiently alleviated in Pad4 KO mice (Fig. 6e). This evidence shed the light to the critical role of NETs in the development of CIPN.

The co-localization of NE, MPO, and endothelial cell marker CD31 indicated that NETs occurred in blood vessels (Supplementary Fig. S7). Together with the evidence of increased HIF-1α in DRG (Fig. 5g), decreased blood flow in extremities and recruitment of ischemic homing peptide in tail and sciatic nerve (Fig. 5d–f), we verified that the microcirculation disturbance in CIPN was caused by NETs. In clinical practice, CIPN can be treated by raising blood pressure and improving circulation. Clinical experience indicated that long wave diathermy treatment (LWD) decreased CIPN symptoms by heightening circulation and heat.[38] What's more,

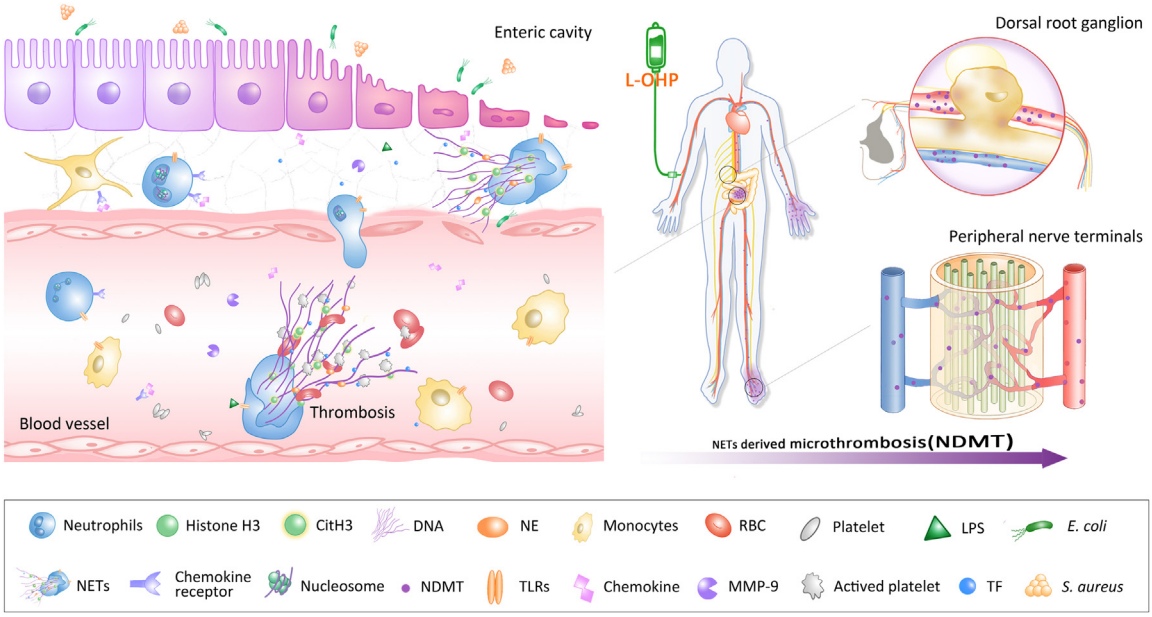

***Fig. 8:* Schematic illustration indicating that chemotherapy-induced NETs contribute to the development of CIPN by disturbing microcirculation.** L-OHP leads to intestinal barrier destruction and inflammatory infiltration, and gut microbe-derived LPS triggers neutrophils to form NETs, which are subsequently released into the blood. NETs-mediated microcirculation disturbance causes ischemia and hypoxia in the DRG and limbs, which contributes to the progression of CIPN.

venlafaxine, a serotonin-norepinephrine reuptake inhibitor, effectively in treating depression has a side effect which can cause modest increase in blood pressure has a benefit in CIPN treatment. It implies that the improvement of circulation could reduce chemotherapy-induced mechanical hyperalgesia.[39] Besides the microthrombus caused by NETs after chemotherapy, eosinophil ETosis could also induce thrombus in small vessels during the development of eosinophilic granulomatosis with polyangiitis.[40] These data indicated that the release of intracellular components from leukocytes in the bloodstream may cause disturbed microcirculation and ischemic status.

Chemotherapy also induced macrophages to express TF.[41] TF is the main trigger of extrinsic coagulation combining with factor VII to induce thrombosis.[6] Chemotherapeutic drugs significantly increased the expression of TF and reduced the expression of TFPI in macrophages, platelets and vascular endothelium.[42] As a high energy consuming tissue, the nervous system is very sensitive to the change in oxygen supply. High expression of TF can induce microthrombus around the peripheral nerve and lead to hypoxia-related molecular events, such as the increase of HIF-1α. As a transcription factor HIF-1α responds to the hypoxia in cellular environment. HIF-1α upregulates the expression of many downstream molecules, such as VEGF and MMPs. It was proved that HIF-1α was widely involved in chronic peripheral nerve sensitization.[7] Our previous studies revealed that TF and HIF-1α participated in the CIPN process.[7] Therefore, we examined whether the inhibition of NETs could affect the expression of TF and HIF-1α. The data indicated that pharmacologic suppressions or genetic ablation of MPO or PAD4 could effectively reduce the levels of TF and HIF-1α in DRG from L-OHP-treated mice (Figs. 5g, 6m and n). It suggested an association between neutrophils activation and microcirculation obstacle in CIPN.

It has been reported that DNase1 is the most important endogenous factor in controlling NETs to prevent vascular occlusion.[14,43] Furthermore, DNase1 has been used clinically without toxicity and side effects being observed.[44] Administration of DNase1 resulted in the degradation of NETs in mice model of breast cancer, lung injury and systemic lupus erythematosus.[44] Our results showed that DNase1 (150U) significantly alleviated the mechanical hyperalgesia induced by L-OHP through improving microcirculation disorder caused by NETs (Fig. 3d). It could increase blood flow of the lower limbs and alleviate the ischemia of sciatic nerve after L-OHP administration (Fig. 3f and g). These also manifested that CIPN was mostly an ischemic disease promoted by NETs. In 2008, a peptide CLEVSRKNC targeting ischemic brain tissue was first reported.[16] Synthetic CLEVSRKNC peptide, which resides in ischemic stroke tissue, can be used as a molecular probe for imaging and deliver drugs to ischemic tissues.[5] Therefore, we coupled CLEVSRKNC (SHp) with

DNase1 and administered it intravascularly to CIPN mice. Our results showed that SHp-DNase1 could improve the peripheral blood flow and relieve the mechanical hyperalgesia more effectively than DNase1 alone (Fig. 7). NETs degradation by DNase1 may have an important clinical significance, considering its effective, safe and extensive application prospect in the treatment of NETs-induced diseases, such as infections, autoimmune diseases, and a variety of cancers. In summary, NETs act as a key element in the development of CIPN, associating the intestinal flora intrusion, microcirculation disturbance and peripheral neuropathy. Targeting NETs to improve local microcirculation in peripheral nerves and extremities offers a new strategy for the treatment of CIPN and its related problems (Fig. 8).

Nevertheless, our study has some limitations. The first is that our study focus on the mechanisms of neuropathy caused by platinum compounds. However, there are multiple mechanisms depending on the individual chemotherapeutic agents. Therefore, the effect of other chemotherapeutic agents (such as taxanes, vinca-alkaloids, bortezomib and thalidomide) on NETosis should be considered in our future study. Another is that DNase from bovine pancreas used may contain contaminating chymotrypsin or proteases. In our future study, we may used chymotrypsin or proteases free DNase to degrade NETs.

Contributors

C. J., W. L., and H. X. designed and supervised the research. C. W., T. L., L. H., L. W., and X. Y. did laboratory experiments. C. J., X. W., X. Z., Y. L., F. H., and H. Y. did performed analyses and collected plasma samples. C. W., C. J., and T. L. wrote the original draft. C. J., C. W., and T. L. verified the data and edited the final draft. All authors read and approved the final version of the manuscript, and ensured it is the case.

Data sharing statement

All data associated with this study are present in the paper or the Supplementary Materials. Any additional information required to reanalyze the data reported in this work paper is available from the lead contact upon request.

Declaration of interests

The authors declare that they have no competing interests.

Acknowledgements

We acknowledge all authors participating in this study. And this study was funded by the National Natural Science Foundation of China 81870870, 81971047, 81773798, 82271252; Natural Science Foundation of Jiangsu Province BK20191253; Major Project of "Science and Technology Innovation Fund" of Nanjing Medical University 2017NJMUCX004; Key R&D Program (Social Development) Project of Jiangsu Province BE2019732; Nanjing Special Fund for Health Science and Technology Development YKK19170.

Appendix A. Supplementary data

Supplementary data related to this article can be found at https://doi.org/10.1016/j.ebiom.2023.104499.

References

1 Park SB, Goldstein D, Krishnan AV, et al. Chemotherapy-induced peripheral neurotoxicity: a critical analysis. *CA Cancer J Clin*. 2013;63:419–437.
2 Seretny M, Currie GL, Sena ES, et al. Incidence, prevalence, and predictors of chemotherapy-induced peripheral neuropathy: a systematic review and meta-analysis. *Pain*. 2014;155:2461–2470.
3 Wolf S, Barton D, Kottschade L, Grothey A, Loprinzi C. Chemotherapy-induced peripheral neuropathy: prevention and treatment strategies. *Eur J Cancer*. 2008;44:1507–1515.
4 LoMonaco M, Milone M, Batocchi AP, Padua L, Restuccia D, Tonali P. Cisplatin neuropathy: clinical course and neurophysiological findings. *J Neurol*. 1992;239:199–204.
5 Lechner D, Weltermann A. Chemotherapy-induced thrombosis: a role for microparticles and tissue factor? *Semin Thromb Hemost*. 2008;34:199–203.
6 Haddad TC, Greeno EW. Chemotherapy-induced thrombosis. *Thromb Res*. 2006;118:555–568.
7 Yang Y, Hu L, Wang C, et al. p38/TF/HIF-α signaling pathway participates in the progression of CIPN in mice. *BioMed Res Int*. 2019;2019:5347804.
8 Innominato PF, Giacchetti S, Moreau T, et al. Prediction of survival by neutropenia according to delivery schedule of oxaliplatin-5-Fluorouracil-leucovorin for metastatic colorectal cancer in a randomized international trial (EORTC 05963). *Chronobiol Int*. 2011;28:586–600.
9 Nakanishi T, Aoki D, Watanabe Y, et al. A Phase II clinical trial of pegylated liposomal doxorubicin and carboplatin in Japanese patients with platinum-sensitive recurrent ovarian, fallopian tube or primary peritoneal cancer. *Jpn J Clin Oncol*. 2015;45:422–426.
10 Brinkmann V, Reichard U, Goosmann C, et al. Neutrophil extracellular traps kill bacteria. *Science*. 2004;303:1532–1535.
11 Lögters T, Paunel-Görgülü A, Zilkens C, et al. Diagnostic accuracy of neutrophil-derived circulating free DNA (cf-DNA/NETs) for septic arthritis. *J Orthop Res*. 2010;27:1401–1407.
12 Papayannopoulos V, Metzler KD, Hakkim A, Zychlinsky A. Neutrophil elastase and myeloperoxidase regulate the formation of neutrophil extracellular traps. *J Cell Biol*. 2010;191:677–691.
13 Geering B, Stoeckle C, Conus S, Simon HU. Living and dying for inflammation: neutrophils, eosinophils, basophils. *Trends Immunol*. 2012;34:398–409.
14 Jiménez-Alcázar M, Rangaswamy C, Panda B, et al. Host DNases prevent vascular occlusion by neutrophil extracellular traps. *Science*. 2017;358:1202–1206.
15 Argyriou AA, Bruna J, Marmiroli P, Cavaletti G. Chemotherapy-induced peripheral neurotoxicity (CIPN): an update. *Crit Rev Oncol Hematol*. 2012;82:51–77.
16 Hong HY, Choi JS, Lee HY, et al. Detection of apoptosis in a rat model of focal cerebral ischemia using a homing peptide selected from in vivo phage display. *J Control Release*. 2008;131:167–172.
17 Lv W, Xu J, Wang X, Li X, Xu Q, Xin H. Bioengineered boronic ester modified dextran polymer nanoparticles as reactive oxygen species responsive nanocarrier for ischemic stroke treatment. *ACS Nano*. 2018;12:5417–5426.
18 Massberg S, Grahl L, von Bruehl Ml, et al. Reciprocal coupling of coagulation and innate immunity via neutrophil serine proteases. *Nat Med*. 2010;16:887–896.
19 Shen S, Lim G, You Z, et al. Gut microbiota is critical for the induction of chemotherapy-induced pain. *Nat Neurosci*. 2017;20:1213–1216.
20 Khan MA, Farahvash A, Douda DN, et al. JNK activation turns on LPS- and gram-negative bacteria-induced NADPH oxidase-dependent suicidal NETosis. *Sci Rep*. 2017;7:3409.
21 Zafarullah M, Li WQ, Sylvester J, Ahmad M. Molecular mechanisms of N-acetylcysteine actions. *Cell Mol Life Sci*. 2003;60:6–20.
22 Fuchs TA, Abed U, Goosmann C, et al. Novel cell death program leads to neutrophil extracellular traps. *J Cell Biol*. 2007;176:231–241.
23 Kolaczkowska E, Jenne CN, Surewaard BG, et al. Molecular mechanisms of NET formation and degradation revealed by intravital imaging in the liver vasculature. *Nat Commun*. 2015;6:6673.
24 Li P, Li M, Lindberg MR, Kennett MJ, Xiong N, Wang Y. PAD4 is essential for antibacterial innate immunity mediated by neutrophil extracellular traps. *J Exp Med*. 2010;207:1853–1862.
25 Han Y, Smith MT. Pathobiology of cancer chemotherapy-induced peripheral neuropathy (CIPN). *Front Pharmacol*. 2013;4:156.
26 Krukowski K, Nijboer CH, Huo X, Kavelaars A, Heijnen CJ. Prevention of chemotherapy-induced peripheral neuropathy by the small-molecule inhibitor pifithrin-μ. *Pain*. 2015;156:2184–2192.
27 Gardiner EE, Andrews RK. Neutrophil extracellular traps (NETs) and infection-related vascular dysfunction. *Blood Rev*. 2012;26:255–259.

28 Engelmann B, Massberg S. Thrombosis as an intravascular effector of innate immunity. *Nat Rev Immunol*. 2013;13:34–45.
29 Jorch SK, Kubes P. An emerging role for neutrophil extracellular traps in noninfectious disease. *Nat Med*. 2017;23:279–287.
30 Miedema KG, de Bont ES, Oude Nijhuis CS, van Vliet D, Kamps WA, Tissing WJ. Validation of a new risk assessment model for predicting adverse events in children with fever and chemotherapy-induced neutropenia. *J Clin Oncol*. 2011;29:e182–e184.
31 Liem L, van Dongen E, Huygen FJ, Staats P, Kramer J. The dorsal root ganglion as a therapeutic target for chronic pain. *Reg Anesth Pain Med*. 2016;41:511–519.
32 Loman BR, Jordan KR, Haynes B, Bailey MT, Pyter LM. Chemotherapy-induced neuroinflammation is associated with disrupted colonic and bacterial homeostasis in female mice. *Sci Rep*. 2019;9:16490.
33 Nakazawa D, Shida H, Tomaru U, et al. Enhanced formation and disordered regulation of NETs in myeloperoxidase-ANCA-associated microscopic polyangiitis. *J Am Soc Nephrol*. 2014;25:990–997.
34 Obermayer A, Stoiber W, Krautgartner WD, et al. New aspects on the structure of neutrophil extracellular traps from chronic obstructive pulmonary disease and in vitro generation. *PLoS One*. 2014;9:e97784.
35 Addington J, Freimer M. Chemotherapy-induced peripheral neuropathy: an update on the current understanding. *F1000Res*. 2016;5:1446.
36 Rochael NC, Guimarães-Costa AB, Nascimento MT, et al. Classical ROS-dependent and early/rapid ROS-independent release of Neutrophil Extracellular Traps triggered by Leishmania parasites. *Sci Rep*. 2015;5:18302.
37 Amulic B, Cazalet C, Hayes GL, Metzler KD, Zychlinsky A. Neutrophil function: from mechanisms to disease. *Annu Rev Immunol*. 2012;30:459.
38 Tonezzer T, Caffaro LAM, Menon KRS, et al. Effects of transcutaneous electrical nerve stimulation on chemotherapy-induced peripheral neuropathy symptoms (CIPN): a preliminary case-control study. *J Phys Ther Sci*. 2017;29:685–692.
39 Piccolo J, Kolesar JM. Prevention and treatment of chemotherapy-induced peripheral neuropathy. *Am J Health Syst Pharm*. 2014;71:19–25.
40 Koike H, Nishi R, Furukawa S, et al. In vivo visualization of eosinophil secretion in eosinophilic granulomatosis with polyangiitis: an ultrastructural study. *Allergol Int*. 2022;71:373–382.
41 Manly DA, Boles J, Mackman N. Role of tissue factor in venous thrombosis. *Annu Rev Physiol*. 2011;73:515–525.
42 Gessler F, Voss V, Seifert V, Gerlach R, Kögel D. Knockdown of TFPI-2 promotes migration and invasion of glioma cells. *Neurosci Lett*. 2011;497:49–54.
43 Buchanan JT, Simpson AJ, Aziz RK, et al. DNase expression allows the pathogen group A Streptococcus to escape killing in neutrophil extracellular traps. *Curr Biol*. 2006;16:396–400.
44 Vogel B, Shinagawa H, Hofmann U, Ertl G, Frantz S. Acute DNase1 treatment improves left ventricular remodeling after myocardial infarction by disruption of free chromatin. *Basic Res Cardiol*. 2015;110:15.